Simulation of fast-flow features of the Fennoscandian ice sheet during the Last Glacial Maximum

Pirjo-Leena FORSSTRÖM,[1] Olli SALLASMAA,[2] Ralf GREVE,[3] Thomas ZWINGER[1]

[1]*CSC — Scientific Computing Ltd, P.O. Box 405, FIN-02101 Espoo, Finland*
E-mail: forsstro@csc.fi
[2]*Geological Survey of Finland, P.O. Box 96, FIN-02151 Espoo, Finland*
[3]*Institut für Mechanik III, Technische Universität Darmstadt, Hochschulstrasse 1, D-64289 Darmstadt, Germany*

ABSTRACT. In order to reconstruct the palaeoglaciation in Fennoscandia and northern Asia during the late-Weichselian ice-age phase, simulations with the dynamic and thermodynamic ice-sheet model SICOPOLIS are carried out. Our focus is on the Last Glacial Maximum (LGM) around 20 kyr BP. Climate forcing is based on mean annual surface temperature and precipitation derived from present data and Palaeoclimatic Modelling Intercomparison Project (PMIP) UKMO2l results for the LGM. These distributions are interpolated via a glacial index defined by the Greenland Icecore Project (GRIP) δ^{18}O record. The extent of the Scandinavian and the Barents ice sheets is reproduced in good agreement with the Quaternary Environments of the Eurasian North (QUEEN) reconstruction, but the Kara Sea and Taymyr Peninsula areas are excessively glaciated. The fast-flow regions derived from the simulations, which are generally connected to regions with a temperate base and temperate ice above, are compared to hypothesized palaeo-ice-stream locations, especially in the Norwegian Channel and the Baltic area. In the Norwegian Channel, temperate basal conditions with temperate ice above prevail and favour fast flow. In the Baltic area, ice-sheet advance is generally accompanied by slow ice velocities ($<200 \, \mathrm{m \, a^{-1}}$). Some temporary fast-flow features occur due to transitional temperate-base conditions, and higher velocities arise in retreat phases.

1. INTRODUCTION

During the Weichselian glacial period, large parts of northern Eurasia have been covered by ice sheets. The Quaternary Environment of the Eurasian North (QUEEN) project has compiled the most up-to-date reconstruction of ice-sheet extent in Eurasia (Svendsen and others, 1999; Thiede and others, 2001). This reconstruction differs from earlier compilations especially in the southern Kara Sea and the Taymyr Peninsula area, which are deduced to have stayed ice-free during the Last Glacial Maximum (LGM) around 20 kyr BP (Svendsen and others, 1999; Polyak and others, 2000; Mangerud and others, 2002). Details of this extent are still debated: Alexanderson and others (2001) conclude that there is evidence of LGM ice in northwest Taymyr, whereas the QUEEN results indicate arid and ice-free conditions. The QUEEN ice-sheet extent is depicted in Figure 1 together with the location of major palaeo-ice streams.

Proxies for local temperature and precipitation during the LGM are sparse. In addition to more global data from Greenland ice cores and deep-sea sediment records, some local proxies based on palaeobotanical evidence are available (Tarasov and others, 1999). These authors conclude that the temperature anomaly (LGM minus present) for the coldest month of the year at 18 kyr BP is largest in areas near Novgorod, in the range −29 to −20°C. From there, the temperature anomaly decreases to the east. In the Taymyr Peninsula and the Kara Sea areas it is −10 to −3°C. The temperature anomaly for the warmest month is approxi-
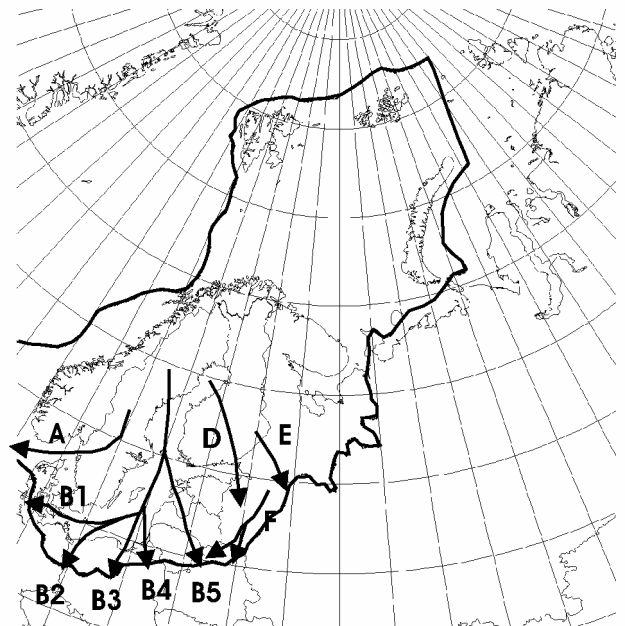

Fig. 1. Ice-sheet extent at LGM (solid line) according to QUEEN (Svendsen and others, 1999; Thiede and others, 2001). Added to this are the approximate positions for the ice streams identified by Boulton and others (2001): the Norwegian Channel ice stream (A), the Baltic Ice Stream (B), the Danish sub-lobe (B1), the Oder sub-lobe (B2), the Wisla sub-lobe (B3), the Kurshkiy sub-lobe (B4), the Riga sub-lobe (B5), the Finnish ice stream (D), the Karelian ice stream (E) and the Novgorod ice stream (F).

mately −3 to 0°C in the whole domain. The anomaly in precipitation rate is −450 to −200 mm a^{-1}.

If these reconstructions are compared to Palaeoclimate Modelling Intercomparison Project (PMIP) results from the United Kingdom Meteorological Office (UKMO) (Hewitt and Mitchell, 1997), we can see that the winter temperature anomaly in southeast regions is in agreement with the results obtained by Tarasov and others (1999). However, the UKMO results show an anomaly of similar magnitude in the northeast, whereas Tarasov and others (1999) state that the LGM climate was warmer in this region.

Simulations of Fennoscandian and related ice sheets have been conducted by Fastook and Holmlund (1994), Peltier (1994), Huybrechts and T'siobbel (1995), Payne and Baldwin (1999) and Siegert and others (1999). Simulations of Northern Hemisphere ice-sheet retreat utilizing atmospheric general circulation model (AGCM) results have been carried out by Charbit and others (2002).

Siegert and others (1999) have utilized the QUEEN project data for ice-sheet extent in their simulations. In their simulation, a zero level of precipitation is set across the Taymyr Peninsula, and resulting reconstructions are then compared with geological evidence. In this way, the most likely glacial scenario is selected.

According to Boulton and others (2001), high flow rates are needed in the Baltic basin to achieve the inferred LGM extent. Several major ice streams are inferred in the area (Boulton and others, 2001; Stokes and Clark, 2001) (Fig. 1). The Norwegian Channel Ice Stream (NCIS) has recently been identified from geological data (e.g. glacially fed fans) (Sejrup and others, 1998, 2000), the Baltic Ice Stream (BIS) and its sub-lobes have been widely discussed (e.g. Kleman and others, 1997) and the Finnish, the Karelian and the Novgorod ice streams are discussed by, for example, Houmark-Nielsen and Humlum (1994), Larsen and others (1999) and Lunkka and others (2001).

2. MODELLING APPROACH

The dynamics and thermodynamics of the Fennoscandian and adjacent glaciation is investigated with the ice-sheet model SICOPOLIS (SImulation COde for POLythermal Ice Sheets; Greve, 1997a, b). The model describes the material ice as an incompressible, heat-conducting, power-law fluid with thermomechanical coupling due to the strong temperature dependence of the flow law,

$$\boldsymbol{D} = EA(T', \omega)\sigma^{n-1}\boldsymbol{t}^{\mathrm{D}}, \qquad (1)$$

where $\boldsymbol{D} = \mathrm{sym\, grad}\,\boldsymbol{v}$ (velocity $\boldsymbol{v}$) is the strain-rate tensor, $\boldsymbol{t}^{\mathrm{D}}$ the Cauchy stress deviator, $\sigma = [\mathrm{tr}(\boldsymbol{t}^{\mathrm{D}})^2/2]^{\frac{1}{2}}$ the effective shear stress, n the power-law exponent and $A(T', \omega)$ the flow-rate factor, which depends exponentially on the temperature T' relative to the pressure-melting point and linearly on the water content ω (see Greve and others, 1998). The flow-enhancement factor E is equal to unity for pure ice and can deviate from unity due to the softening or stiffening effect of impurities in the ice.

Cold ice with a temperature below the pressure-melting point is distinguished from *temperate ice* with a temperature at the pressure-melting point, the latter being considered as a binary mixture of ice and small amounts of water. The interface that separates cold and temperate ice is monitored using Stefan-type energy-flux and mass-flux matching conditions. Basal sliding is assumed to be zero for a cold base,

and for a temperate base it is described by the Weertman-type sliding law in the form of Greve and others (1998),

$$\boldsymbol{v}_{\mathrm{sl}} = -C_{\mathrm{sl}}H\|\mathrm{grad}\,h\|^2\,\mathrm{grad}\,h, \qquad (2)$$

where $\boldsymbol{v}_{\mathrm{sl}}$ is the basal sliding velocity, C_{sl} the sliding coefficient, H the ice thickness and h the surface elevation.

The model computes the three-dimensional temporal evolution of the ice extent, thickness, velocity, temperature, water content and age in response to external forcing. The latter must be specified by (i) the mean annual air temperature at the ice surface, (ii) the surface mass balance, which is ice accumulation (here assumed to be snowfall) minus ablation (here assumed to be melting), (iii) the global sea level and (iv) the geothermal heat flux entering the ice mass from below. Isostatic depression and rebound of the lithosphere due to changing ice loads is described by a local-lithosphere-relaxing-asthenosphere (LLRA) model with the isostatic time lag τ_{iso} (Le Meur and Huybrechts, 1996; Greve, 2001). A more detailed description of the model is given by Greve (1997a, b).

Since SICOPOLIS is based on the shallow-ice approximation (SIA), it neglects normal stress deviators and shear stresses in vertical planes. The large-scale behaviour of ice sheets is simulated well with the SIA; however, it is not valid locally in the vicinity of ice domes and close to the margin. Further, fast-flowing ice streams with reduced basal drag are not adequately described by the SIA. Nevertheless, SICOPOLIS can produce fast-flow features which arise from sliding over a temperate ice base (Equation (2)). These fast-flow features can resemble real ice streams, but as no specific ice-stream dynamics is included, they are a coarse approximation of the real dynamics.

Ice shelves are not treated explicitly. Instead, the ice sheet is allowed to glaciate the continental shelf below sea level, provided the seabed elevation is larger than a threshold value z_{thresh}. This parameter was introduced in order to prevent the ice sheet from glaciating the deep sea, which is of course not realistic.

The areal coverage in our simulations is from the North Atlantic to the Taymyr Peninsula, and covers an area of $3680 \times 3800\,\mathrm{km}^2$. This area was chosen such that it covers the reconstructed ice-sheet extent in the east. Any artificial ice-sheet growth further to the east is finally cut off by the margin of the domain. A clear shortcoming of this set-up is that the British Isles are not yet included; this will be done for future simulations. The stereographic projection with a reference latitude of 71° is applied. The grid spacing for the simulations in horizontal direction is 40 km, leading to a total of 93×96 gridpoints. The vertical resolution is 21 gridpoints in the cold-ice region, 11 gridpoints in the temperate-ice region (if existing) and 11 gridpoints in the lithosphere (Greve, 1997b).

Simulation time is from 250 kyr BP to the present, of which the first approximately 50 kyr are required for spin-up (that is, for losing the memory of the arbitrarily chosen ice-free initial conditions). Even as our main focus is on the reconstruction of the LGM around 20 kyr BP, the dynamics of the whole Weichselian glaciation is of interest. Also, the ice-load history is important for the bedrock elevation due to the isostatic time lag. Values of physical parameters are listed in Table 1.

3. CLIMATIC FORCING

In order to provide modern surface temperature and pre-

Table 1. Physical parameters of the ice-sheet model

Quantity	Value
Gravity acceleration, g	$9.81\,\mathrm{m\,s^{-2}}$
Density of ice, ρ	$910\,\mathrm{kg\,m^{-3}}$
Power-law exponent, n	3
Flow-enhancement factor, E	3
Heat conductivity of ice, κ	$9.828\,e^{-0.0057T[\mathrm{K}]}\,\mathrm{W\,m^{-1}\,K^{-1}}$
Specific heat of ice, c	$(146.3+7.253T[\mathrm{K}])\,\mathrm{J\,kg^{-1}\,K^{-1}}$
Latent heat of ice, L	$335\,\mathrm{kJ\,kg^{-1}}$
Clausius–Clapeyron gradient, β	$8.7\times10^{-4}\,\mathrm{K\,m^{-1}}$
Geothermal heat flux, q_{geo}	$55\,\mathrm{mW\,m^{-2}}$
Threshold seabed elevation for glaciation, z_{thresh}	$-400\,\mathrm{m}$
Isostatic time lag, τ_{iso}	3000 years
Asthenosphere density, ρ_{a}	$3300\,\mathrm{kg\,m^{-3}}$
Density × specific heat of the lithosphere, $\rho_{\mathrm{r}}c_{\mathrm{r}}$	$2000\,\mathrm{kJ\,m^{-3}\,K^{-1}}$
Heat conductivity of the lithosphere, κ_{r}	$3\,\mathrm{W\,m^{-1}\,K^{-1}}$

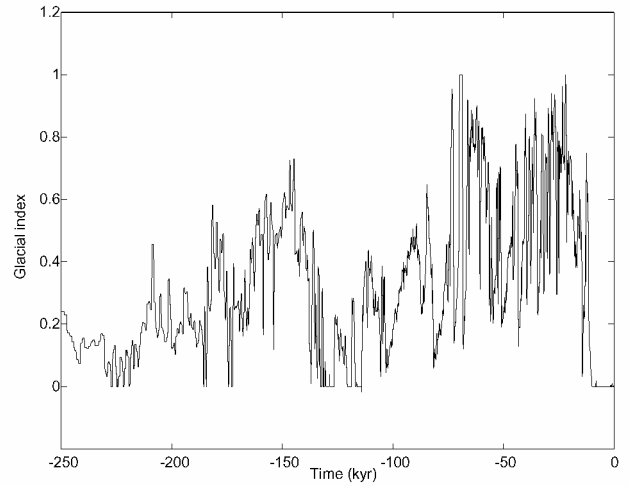*Fig. 2. Glacial index $g(t)$ as a function of time. This index scales the GRIP $\delta^{18}O$ record (Dansgaard and others, 1993) to represent glacial ($g=1$) and present ($g=0$) conditions.*

cipitation values, measured and modelled datasets by Legates and Willmott (1990) are used. These data have been gathered from the Global Historical Climatology Network (Vose and others, 1992) and station records for the years 1950–96. The source resolution is $0.5°\times0.5°$, and the data are interpolated for each season with inverse-distance weighing to the 40 km grid of SICOPOLIS.

Our first attempt to parameterize past climate conditions was similar to the method applied by Greve and others (1999). Past temperatures were calculated from present values with a conversion formula that takes into account that climate is generally warmer or colder, and that the surface elevation has changed. However, this approach leads inevitably to a very extensive glaciation because it does not account for different spatial patterns of LGM and present climate conditions, and is therefore not suitable for a detailed study of Eurasian glaciation.

In the current approach, values for temperature and precipitation from the UKMO21 LGM simulations (Hewitt and Mitchell, 1997) are utilized. The UKMO21 dataset was chosen from comparisons of ice-sheet mass budgets in the PMIP simulations (Pollard and others, 2000). The coarse atmospheric model output was again interpolated with inverse-distance weighting to the model grid.

The seasonal temperature and precipitation distributions are then interpolated linearly between the present (Legates and Willmott, 1990) and LGM (UKMO21) values with a glaciation index $g(t)$. This index scales the Greenland Icecore Project (GRIP) $\delta^{18}O$ record (Dansgaard and others, 1993) to represent LGM ($g=1$) and present ($g=0$) conditions (Fig. 2). The interpolation is carried out by

$$f(x,y,t) = (1-g(t))f_{\mathrm{present}}(x,y) + g(t)f_{\mathrm{LGM}}(x,y), \quad (3)$$

where x and y are Cartesian coordinates which span the stereographic plane, t is the time, f is the surface temperature or precipitation, and $f_{\mathrm{present}}(x,y)$ and $f_{\mathrm{LGM}}(x,y)$ are the spatially resolved data for the two time-slices, respectively. Conversion from seasonal precipitation P to seasonal snowfall (solid precipitation) S is done with the empirical relation by Marsiat (1994),

$$S = P \times \begin{cases} 0, & T_{\mathrm{s}} \geq 7°\mathrm{C}, \\ (7°\mathrm{C}-T_{\mathrm{s}})/17°\mathrm{C} & -10°\mathrm{C} \leq T_{\mathrm{s}} \leq 7°\mathrm{C}, \\ 1, & T_{\mathrm{s}} \leq -10°\mathrm{C}, \end{cases} \quad (4)$$

where T_{s} is the seasonal surface temperature. Mean annual air temperature is the mean of seasonal temperatures.

Climatic forcing is completed by the degree-day method for surface melting in the form presented by Reeh (1991) (parameters: degree-day factor for snowmelt $\beta_{\mathrm{snow}} = 3\,\mathrm{mm\,w.e.\,d^{-1}\,°C^{-1}}$; degree-day factor for ice melt $\beta_{\mathrm{ice}} = 12\,\mathrm{mm\,w.e.\,d^{-1}\,°C^{-1}}$; saturation factor for the formation of superimposed ice $P_{\mathrm{max}} = 0.6$; standard deviation of short-term, statistical air-temperature fluctuations $\sigma_{\mathrm{stat}} = 5°\mathrm{C}$), sea-level changes derived from the spectral-mapping project (SPECMAP) record (Imbrie and others, 1984) and the global-mean value $q_{\mathrm{geo}} = 55\,\mathrm{mW\,m^{-2}}$ for the geothermal heat flux.

4. RESULTS

4.1. Ice-sheet extent and thickness

At the LGM around 20 kyr BP, the simulated ice sheet (Fig. 3)

Fig. 3. The simulated ice-sheet extent (thick solid line) and thickness (solid contours, spacing 1 km) at the LGM (20 kyr BP). The thick dashed line indicates the LGM ice-sheet extent by QUEEN (Svendsen and others, 1999; Thiede and others, 2001).
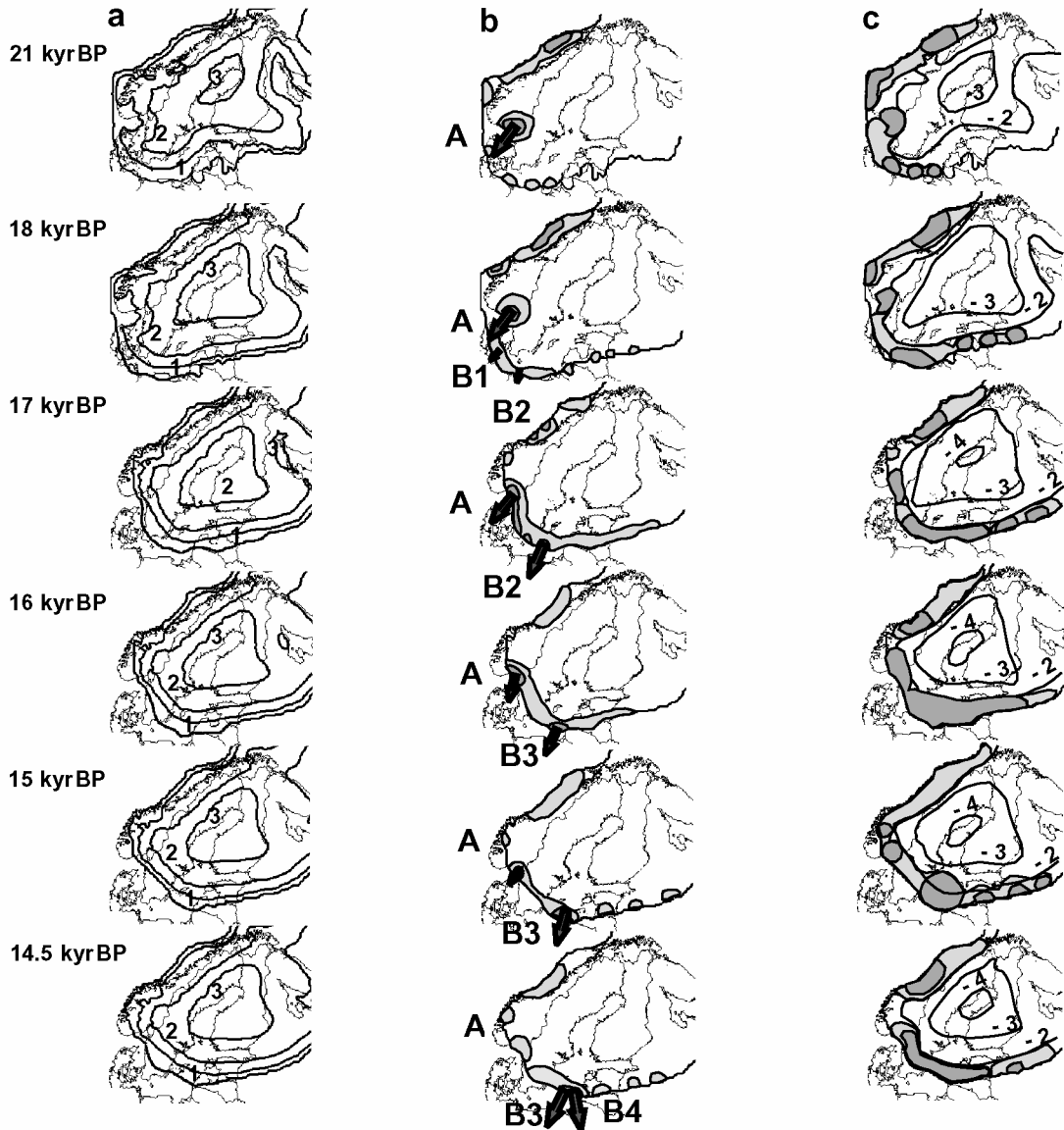
Fig. 4. Simulation results for the Norwegian Channel and Baltic Basin ice-stream activity at 21, 18, 17, 16, 15 and 14.5 kyr BP. A and B1–B4 are simulated positions of fast-flow features. (a) Ice-sheet thickness (contour spacing 1 km). (b) Flow velocity. For white areas $|\boldsymbol{v}| < 200\,\mathrm{m\,a^{-1}}$; for light shading $200\,\mathrm{m\,a^{-1}} \leq |\boldsymbol{v}| < 300\,\mathrm{m\,a^{-1}}$; for dark shading $300\,\mathrm{m\,a^{-1}} \leq |\boldsymbol{v}| < 400\,\mathrm{m\,a^{-1}}$; for short arrows $400\,\mathrm{m\,a^{-1}} \leq |\boldsymbol{v}| < 700\,\mathrm{m\,a^{-1}}$; for mid-length arrows $700\,\mathrm{m\,a^{-1}} \leq |\boldsymbol{v}| < 1000\,\mathrm{m\,a^{-1}}$; for long arrows $|\boldsymbol{v}| \geq 1000\,\mathrm{m\,a^{-1}}$. (c) Basal temperature in °C. Dark (light) shading indicates a temperate base with temperate (cold) ice above. In all panels, the outermost contour shows the ice margin.

shows two different parts, namely, the Fennoscandian and the Barents–Kara ice sheets. The Fennoscandian ice sheet lies within its geologically reconstructed boundaries, but the eastern part is heavily over-glaciated in the Kara Sea and Taymyr areas. The total areal coverage of the Eurasian glaciation is $7.4 \times 10^6\,\mathrm{km^2}$, and the sea-level equivalent at that date is 39.5 m. If we compare this to the estimates of ice-equivalent sea levels for the LGM ice sheet by Clark and Mix (2002), we notice that the maximum Climate Long-Range Investigation Mapping and Prediction (CLIMAP) value for the Fennoscandian and Barents area ice sheets is 34.0 m. This is over 5 m lower than our result. However, looking at our resulting ice-sheet topography at the LGM, we notice that the over-glaciated eastern section makes a major contribution to the ice-sheet volume. The simulated maximum ice-sheet thickness in Fennoscandia at the LGM, approximately 3 km, is reached over the Gulf of Bothnia.

The PMIP results including UKMO2l utilize the ICE-4G ice-sheet data (Peltier, 1994), which have the best available spa-tial resolution. The PMIP runs are thus based on a heavily glaciated Eurasia which is not supported by the QUEEN reconstruction. It is likely that this leads to biased LGM temperatures which, in turn, are responsible for the over-glaciated Eurasian Arctic of our simulation.

An inverse approach has been used to determine the climate parameters (temperature, precipitation) in order to fit the modelled ice-sheet extent to the QUEEN observations. Preliminary results indicate that if the climate forcing defined by Equations (3) and (4) is modified such that winter precipitations are limited to $150\,\mathrm{mm\,a^{-1}}$ and, simultaneously, summer temperatures are kept above 3°C during the glacial, the eastern Eurasian part will not be glaciated. This approach will be investigated in more detail in a future study.

4.2. Ice streams

By definition, an ice stream is a region of grounded ice which flows much faster than the surrounding ice on either side

(Paterson, 1994). The main references for palaeo-ice streams are Denton and Hughes (1981) and Stokes and Clark (2001). In these studies, the hypothesized palaeo-ice-stream locations are identified (see also Fig. 1). The main ice streams were marine, as nowadays in Antarctica and Greenland. However, terrestrial ice streams were active at glacial times as well (e.g. the inferred BIS (Punkari, 1993, 1997)).

The modelled fast-flow features in our simulations (Fig. 4b) can be seen as coarse approximations of real ice streams. However, it must be kept in mind that, first, the 40 km model grid is too coarse to resolve the small width of real ice streams, and second, as mentioned above, the model uses the shallow-ice approximation which does not include the particular ice-stream physics. In our model, fast flow arises from basal sliding over a temperate base and is therefore favoured by steep surface gradients and topographic depressions of the bedrock where the ice is thick.

We obtain fast-flow regions at St Anna Trough, Franz Josef Trough, Bear Island Trough, the Trondheim area and the Norwegian Channel. These are located in topographic troughs, where the base is temperate (Fig. 4c), and they coincide with locations of marine-based ice streams indicated by geologic evidence (see section 1).

Terrestrial ice streams were inferred for the Baltic area in several stages of glaciation at varying locations (see section 1). In our simulation, ice flow is generally slow in the Baltic area during the advance phase of the ice sheet. However, during the retreat phase after the LGM a temperate ice base forms in that region, and ice flow is significantly accelerated.

The threshold seabed elevation on the continental shelf which is allowed to glaciate (z_{thresh}) is a sensitive determinant of modelled maritime ice-stream locations. Therefore, it is important to choose an appropriate value for this parameter, which was achieved by matching simulated and reconstructed marine ice-sheet margins at the LGM (Fig. 3). Otherwise, maritime ice-stream locations are quite robust to changed input parameters. By contrast, terrestrial ice-stream locations differ significantly with different parameter sets.

5. DISCUSSION

5.1. Norwegian Channel area

The Norwegian Channel ice stream (NCIS) is regarded as important for the Fennoscandian ice-sheet dynamics (Stokes and Clark, 2001). The activity of the NCIS has been discussed by Sejrup and others (1998, 2000), who conclude that the NCIS was active during the periods 50–40, 28–22 and 18–15 kyr BP. Between these periods, the stability and duration of the stream activity is not known. These results are based on lithology, biostratigraphy and geochronological investigations.

The results of our simulation for six time-slices are shown in Figure 4. Evidently, fast flow prevails in the NCIS area (A; Fig. 4). It occurs first at 28 kyr BP, with high surface velocities of 1400 m a^{-1} in the Norwegian Channel, the velocity near the base being approximately 1000 m a^{-1}. The NCIS is situated near the margin of the ice sheet, with a large surface gradient, and there is a temperate base with temperate ice above. The period 28–18 kyr BP is rather stable in our simulation, with fast ice flow from the northeast to the southwest. The area with a temperate base overlain by a temperate-ice layer is rather constant (around 20 000 km^2), with minor areal changes that do not affect the fast flow.

At 18 kyr BP, the simulated ice sheet starts thinning in the western section. There is a large area around southern Sweden with temperate-base conditions but cold ice above. There the velocities are approximately 400–700 m a^{-1}.

At 17 kyr BP the simulated NCIS fast-flow area has widened, but the peak velocity has diminished to 900 m a^{-1}. At this time, there are some shifts on the main fast-flow direction to the south. After this, the temperate-base area diminishes considerably. The last time when there is fast flow with an ice sheet terminating in water and velocities of about 500 m a^{-1} is at 15 kyr BP. Thereafter, the flow is slowly fading, with velocities of 300 m a^{-1}.

In our simulation, the fast flow in the NCIS area is due to temperate basal conditions and resulting basal sliding. From 28 to 17 kyr BP there is a temperate base with temperate ice above in the Norwegian Channel. As the ice sheet thins, the temperate ice above the base first becomes cold as cold ice flows in from the mountains. As the ice sheet thins further, the temperate base disappears and fast flow ceases.

5.2. Baltic region

The simulated BIS (Fig. 4) has an extensive spatial and temporal dimension. The fast-flow regions coarsely agree with the ice streams described by Boulton and others (2001). In our results, lobate structures form when ice is flowing to topographic depressions.

The main simulated advance towards the southern-Sweden/Denmark region starts around 24 kyr BP. At this time, there is a temperate base with cold ice above at the ice-sheet margin in southern Sweden, and the ice sheet ends in the sea. The velocities are approximately 200 m a^{-1}. There is stable thickening of the ice sheet until 19 kyr BP, with alternating temperate and cold ice above a temperate base near the margin. At 19 kyr BP the ice in the marginal areas is warm and mobile, with typical velocities around 600 m a^{-1}. From then on, the ice sheet quickly retreats. Nevertheless, and in contrast to the NCIS, the simulated BIS is still active after 15 kyr BP. Velocities of up to 700 m a^{-1} are maintained, and occasionally peak values of > 1000 m a^{-1} are reached.

The simulated fast-flow features connected to separate sub-lobes develop in the following way:

The Danish sub-lobe (B1) advances steadily at 24 kyr BP from areas west of the Baltic Basin with low velocities. At 18 kyr BP it starts to retreat. The ice-flow velocity at this time is approximately 600 m a^{-1}, and there is a wide marginal area (B1–B3) with temperate base and temperate ice above.

The Oder sub-lobe (B2) advances at 23 kyr BP. The flow starts to accelerate at 18 kyr BP, starting from approximately 600 m a^{-1}, and attains a peak of 1200 m a^{-1} at 17 kyr BP. This is due to the temperate marginal conditions.

The Wisla sub-lobe (B3) advances at 23 kyr BP. Temperate basin appears in the area at 18 kyr BP, increasing the ice flow. The velocity is 900 m a^{-1} at 16 kyr BP, 1000 m a^{-1} at 15 kyr BP and 1400 m a^{-1} at 14.5 kyr BP.

The Kurshkiy sub-lobe (B4) advances to a maximum position at 21 kyr BP, and has the highest-velocity phase at 14.5 kyr BP, with values of 1400 m a^{-1}.

During the ice-margin retreat, the former advance-phase lobate structure is coarsely preserved. When the ice sheet decreases at 16 kyr BP and the southwestern part ends

387

in the sea, a large ice front is mobilized. A periglacial lake is formed in the Baltic basin at 13 kyr BP. This gives rise to a few fast-flow areas (1800 m a^{-1}) at the ice margin.

6. CONCLUSION

The following conclusions can be drawn from our modelling study:

The extent of the Fennoscandian LGM ice sheet is reasonably reconstructed by our simulation.

In the Kara Sea and Taymyr areas, the glaciation obtained is too extensive. Evidently, in these regions the applied climate forcing is not valid. Therefore, in future work we will seek to use general circulation model (GCM) results for the glacial climate based on the QUEEN instead of the ICE-4G ice-sheet extent. Further, in order to minimize the influence of systematic GCM errors, the glacial climate input will be based on anomalies from GCM results (LGM minus present) instead of absolute GCM output.

Despite the model limitations of the 40 km grid and the simplified ice-sheet dynamics, observed main ice-stream locations can be identified as fast-flow features in the simulation results, and they compare well with the geological evidence.

The modelled fast-flow features arise from basal sliding over a temperate base. This is favoured by, but not necessarily dependent on, topographic depressions of the bedrock.

The lobate structure in our results is a result of the advance phase. The lobate structure is preserved in the following decay phase.

The model domain should be increased for future simulations in order to include the British Isles and to extend further to the east.

ACKNOWLEDGEMENTS

REFERENCES

Alexanderson, H., C. Hjort, P. Möller, O. Antonov and M. Pavlov. 2001. The North Taymur ice-marginal zone, Arctic Siberia — a preliminary overview and dating. *Global Planet. Change*, **31**(1–4), 427–445.

Boulton, G. S., P. W. Dongelmans, M. Punkari and M. Broadgate. 2001. Paleoglaciology of and ice sheet through a glacial cycle: the European ice sheet through the Weichselian. *Quat. Sci. Rev.*, **20**(4), 591–625.

Charbit, S., C. Ritz and G. Ramstein. 2002. Simulations of Northern Hemisphere ice-sheet retreat: sensitivity to physical mechanisms involved during the last deglaciation. *Quat. Sci. Rev.*, **21**(1–3), 243–265.

Clark, P. U. and A. C. Mix. 2002. Ice sheets and sea level of the Last Glacial Maximum. *Quat. Sci. Rev.*, **21**, 1–7.

Dansgaard, W. *and 10 others*. 1993. Evidence for general instability of past climate from a 250-kyr ice-core record. *Nature*, **364**(6434), 218–220.

Denton, G. H. and T. J. Hughes. 1981. The Arctic ice sheet: an outrageous hypothesis. *In* Denton, G. H. and T. J. Hughes, *eds. The last great ice sheets*. New York, etc., John Wiley and Sons, 437–467.

Fastook, J. L. and P. Holmlund. 1994. A glaciological model of the Younger Dryas event in Scandinavia. *J. Glaciol.*, **40**(134), 125–131.

Greve, R. 1997a. Application of a polythermal three-dimensional ice sheet model to the Greenland ice sheet: response to steady-state and transient climate scenarios. *J. Climate*, **10**(5), 901–918.

Greve, R. 1997b. A continuum-mechanical formulation for shallow polythermal ice sheets. *Philos. Trans. R. Soc. London, Ser. A*, **355**(1726), 921–974.

Greve, R. 2001. Glacial isostasy: models for the response of the Earth to varying ice loads. *In* Straughan, B., R. Greve, H. Ehrentraut and Y. Wang, *eds. Continuum mechanics and applications in geophysics and the environment*. Berlin, etc., Springer-Verlag, 307–325.

Greve, R., M. Weis and K. Hutter. 1998. Palaeoclimatic evolution and present conditions of the Greenland ice sheet in the vicinity of Summit: an approach by large-scale modelling. *Palaeoclimates*, **2**(2–3), 133–161.

Greve, R., K.-H. Wyrwoll and A. Eisenhauer. 1999. Deglaciation of the Northern Hemisphere at the onset of the Eemian and Holocene. *Ann. Glaciol.*, **28**, 1–8.

Hewitt, C. D. and J. F. B. Mitchell. 1997. Radiative forcing and response of a GCM to ice age boundary conditions: cloud feedback, and climate sensitivity. *Climate Dyn.*, **13**(11), 821–834.

Houmark-Nielsen, M. and O. Humlum. 1994. High deglaciation rates in Denmark during the Late Weichselian — implications for the palaeoenvironment. *Geogr. Tidsskr.*, **94**, 26–27.

Huybrechts, P. and S. T'siobbel. 1995. Thermomechanical modelling of Northern Hemisphere ice sheets with a two-level mass-balance parameterization. *Ann. Glaciol.*, **21**, 111–116.

Imbrie, J. *and 8 others*. 1984. The orbital theory of Pleistocene climate: support from a revised chronology of the marine δ^{18}O record. *In* Berger, A., J. Imbrie, J. Hays, G. Kukla and B. Saltzman, *eds. Milankovitch and climate: understanding the response to astronomical forcing. Part 1*. Dordrecht, etc., D. Reidel Publishing Co., 269–305. (NATO ASI Series C: Mathematical and Physical Sciences 126.)

Kleman, J., C. Hättestrand, I. Borgström and A. Stroeven. 1997. Fennoscandian palaeoglaciology reconstructed using a glacial geological inversion model. *J. Glaciol.*, **43**(144), 283–299.

Larsen, E. *and 6 others*. 1999. Age and extent of the Scandinavian ice sheet in northwest Russia. *Boreas*, **28**(1), 115–132.

Legates, D. R. and C. J. Willmott. 1990. Mean seasonal and spatial variability in global surface air temperature. *Theor. Appl. Climatol.*, **41**, 11–21.

Le Meur, E. and P. Huybrechts. 1996. A comparison of different ways of dealing with isostasy: examples from modelling the Antarctic ice sheet during the last glacial cycle. *Ann. Glaciol.*, **23**, 309–317.

Lunkka, J. P., M. Saarnisto, V. Gey, I. Demidov and V. Kiselova. 2001. Extent and age of the Last Glacial Maximum in the south-eastern sector of the Scandinavian ice sheet. *Global Planet. Change*, **31**(1–4), 407–425.

Mangerud, J., V. Astakov and J.-I. Svendsen. 2002. The extent of the Barents–Kara ice sheet during the Last Glacial Maximum. *Quat. Sci. Rev.*, **21**(1–3), 111–119.

Marsiat, I. 1994. Simulation of the Northern Hemisphere continental ice sheets over the last glacial–interglacial cycle: experiments with a latitude–longitude vertically integrated ice sheet model coupled to a zonally averaged climate model. *Palaeoclimates*, **1**(1), 59–98.

Paterson, W. S. B. 1994. *The physics of glaciers. Third edition*. Oxford, etc., Elsevier.

Payne, A. J. and D. J. Baldwin. 1999. Thermomechanical modelling of the Scandinavian ice sheet: implications for ice-stream formation. *Ann. Glaciol.*, **28**, 83–89.

Peltier, W. R. 1994. Ice age paleotopography. *Science*, **265**(5169), 195–201.

Pollard, D. and PMIP Participating Groups. 2000. Comparisons of ice sheet surface mass budgets from Paleoclimate Modeling Intercomparison Project (PMIP) simulations. *Global Planet. Change*, **24**(2), 79–106.

Polyak, L., M. Levitan, V. Gataullin, T. Khusid, V. Mikhailov and V. Mukhina. 2000. The impact of glaciation, river discharge and sea-level change on Late Quaternary environments in the southwestern Kara Sea. *Intern. J. Earth Sci.*, **89**(3), 550–562.

Punkari, M. 1993. Modelling of the dynamics of the Scandinavian ice sheet using remote sensing and GIS methods. *In* Aber, J. S., *ed. Glaciotectonics and mapping glacial deposits*. Regina, Saskatchewan, Canadian Plains Research Center, University of Regina, 232–250.

Punkari, M. 1997. Glacial and glaciofluvial deposits in the interlobate areas of the Scandinavian Ice Sheet. *Quat. Sci. Rev.*, **16**(7), 741–753.

Reeh, N. 1991. Parameterization of melt rate and surface temperature on the Greenland ice sheet. *Polarforschung*, **59**(3), 1989, 113–128.

Sejrup, H. P., J. Y. Landvik, E. Larsen, J. Janocks, J. Eiriksson and E. King. 1998. The Jaeren area, a border zone of the Norwegian Channel ice stream. *Quat. Sci. Rev.*, **17**(9–10), 801–812.

Sejrup, H. P., E. Larsen, J. Landvik, E. L. King, H. Haflidason and A. Nesje. 2000. Quaternary glaciations in southern Fennoscandia: evidence from southwestern Norway and the northern North Sea region. *Quat. Sci. Rev.*, **19**(7), 667–685.

Siegert, M. J., J. A. Dowdeswell and M. Melles. 1999. Late Weichselian glaciation of the Russian High Arctic. *Quat. Res.*, **52**(3), 273–285.

Stokes, C. R. and C. D. Clark. 2001. Palaeo-ice streams. *Quat. Sci. Rev.*, **20**(13), 1437–1457.

Svendsen, J. I. *and 13 others*. 1999. Maximum extent of the Eurasian ice sheets in the Barents and Kara Sea region during the Weichselian. *Boreas*, **28**(1), 234–242.

Tarasov, P. E. *and 9 others*. 1999. Last Glacial Maximum climate of the former Soviet Union and Mongolia reconstructed from pollen and plant microfossil data. *Climate Dyn.*, **15**(3), 227–240.

Thiede, J., H. A. Bauch, C. Hjort and J. Mangerud. 2001. The Late Quaternary stratigraphy and environments of northern Eurasia and the adjacent Arctic seas — new contributions from QUEEN. *Global Planet. Change*, **31**(1–4), complete volume.

Vose, R. S. *and 6 others*. 1992. *The global historical climatology network: long-term monthly temperature, precipitation, sea level pressure, and station pressure data.* Oak Ridge, TN, Oak Ridge National Laboratory. Carbon Dioxide Information Analysis Center. (Environmental Sciences Division Publication 3912, CDIAC 53, NDP-041.)